

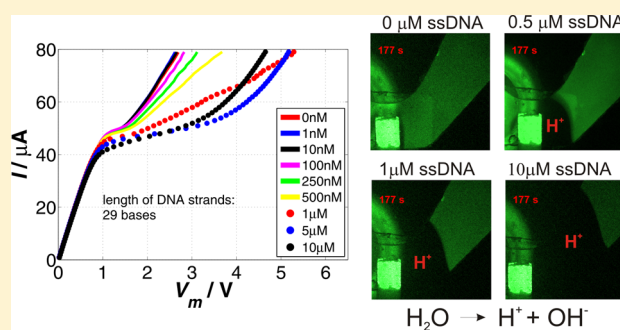
Charge Inversion, Water Splitting, and Vortex Suppression Due to DNA Sorption on Ion-Selective Membranes and Their Ion-Current Signatures

Zdenek Slouka, Satyajyoti Senapati, Yu Yan, and Hsueh-Chia Chang*

Department of Chemical and Biomolecular Engineering, University of Notre Dame, Notre Dame, Indiana 46556, United States

Supporting Information

ABSTRACT: The physisorption of negatively charged single-stranded DNA (ssDNA) of different lengths onto the surface of anion-exchange membranes is sensitively shown to alter the anion flux through the membrane. At low surface concentrations, the physisorbed DNAs act to suppress an electroconvection vortex instability that drives the anion flux into the membrane and hence reduce the overlimiting current through the membrane. Beyond a critical surface concentration, determined by the total number of phosphate charges on the DNA, the DNA layer becomes a cation-selective membrane, and the combined bipolar membrane has a lower net ion flux, at low voltages, than the original membrane as a result of ion depletion at the junction between the cation- (DNA) and anion-selective membranes. However, beyond a critical voltage that is dependent on the ssDNA coverage, water splitting occurs at the junction to produce a larger overlimiting current than that of the original membrane. These two large opposite effects of polyelectrolyte counterion sorption onto membrane surfaces may be used to eliminate limiting current constraints of ion-selective membranes for liquid fuel cells, dialysis, and desalination as well as to suggest a new low-cost membrane surface assay that can detect and quantify the number of large biomolecules captured by probes functionalized on the membrane surface.



INTRODUCTION

Ion-exchange membranes (IEMs) are extensively used in separation processes, mostly in electrodialysis and electro-deionization.¹ These membranes show a unique property of selective ion transport through the nanopores of IEMs embedded with a fixed charge that allows only counterions (ions with opposite charge to that of the fixed one) to pass through as co-ions experience electrostatic repulsion. The ion-exchange membranes are classified as cation- or anion-exchange membranes on the basis of their ability to exchange cations or anions, respectively. Both anion- and cation-exchange membranes display nonlinear current–voltage characteristics (CVC) with three distinguishable regions (Figure 1, left).^{2,3} The first region referred to as the under-limiting region occurs at low voltages where the electrical current is directly proportional to the voltage applied across the membrane, as in the case of an ohmic resistor. The electrical current, however, starts to saturate at a limiting current beyond a critical cross-membrane voltage drop as a result of the ion-transport limitation introduced by ion depletion on one side of the membrane^{4,5}. Ben and Chang⁶ and Yossifon et al.⁷ have shown that the current does not really saturate this limiting region (LR) but is rather a linear function of voltage with a large local differential resistance due to an extended polarized region with space charge at the membrane surface whose existence was first suggested by Rubinstein and Shtilman.² However, an inflection

point appears on the CVC curve at a critical voltage, corresponding to the end of the LR, and the electrical current rises abruptly, giving rise to a second linear region called the overlimiting region (OR).

Although the nonlinear behavior of IEMs was described more than six decades ago,^{8,9} the overlimiting region has been a puzzle and a subject of intensive debate for the last couple of decades. Several mechanisms have been suggested, and the most recent one involves the deionization of the membrane due to an acid–base reaction triggered by the low-pH condition during concentration polarization.¹⁰ However, for most commercial membranes, including the ones used here, chemical stability is essential, so the functional groups are carefully designed to prevent such deionization. The permselectivity of a membrane (Neosepta AMX, Japan) similar to the one used in our work was shown to remain constant after prolonged use,¹¹ and the loss of selectivity cannot explain the occurrence of the OR. The overlimiting current has also been attributed to the following effects:^{12,13} (i) a water-splitting reaction taking place at the interface between the membrane and the depletion zone, (ii) electroconvection (electro-driven vortices) mixing the depletion zone with the conductive bulk of the electrolyte,

Received: February 25, 2013

Revised: April 23, 2013

Published: June 6, 2013

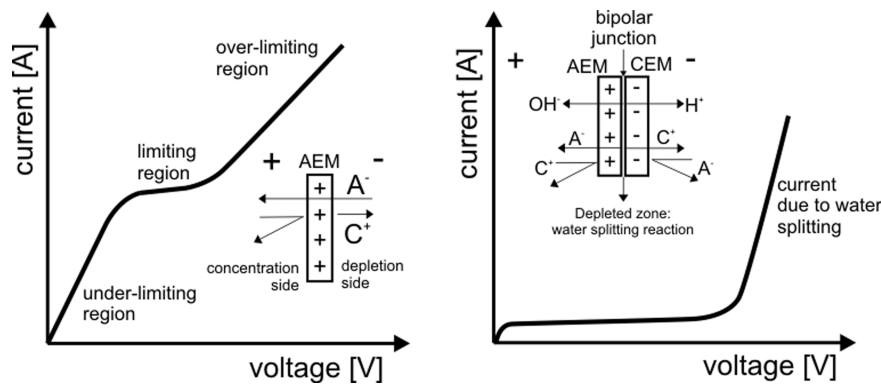


Figure 1. Current–voltage characteristics of an anion-exchange membrane (left) and a bipolar membrane under reverse bias (right) with the schematics showing the transport of cations (C^+) and anions (A^-).

(iii) density gradients developing near the membrane resulting in the transport of the electrolyte due to natural convection, (iv) the exaltation effect associated with water splitting when the H^+ and OH^- ions generated in the depletion region cause an increase in concentration of the other salt ions, and (v) surface conductance and electro-osmotic flow due to a like-charge channel.^{14,15} The true picture may be given by the mutual interplay of these effects¹⁶ or by the dominance of one effect over the other, although surface conductance and electro-osmotic mechanisms can be ruled out in our system with large microchannels with a small surface charge that is opposite from that of the membrane charge. The dominance of one effect could be due to the geometry of the experimental setup and the experimental conditions.¹⁷ However, electroconvection is still considered to be the main mechanism contributing to this overlimiting current^{18–20} and was shown to be affected by the properties of the membranes, such as the membrane charge density,²¹ hydrophobicity,²² conductive heterogeneity,^{23,24} surface heterogeneity of the membrane,¹² or Stokes' radius of the counterions in the electrolyte.²⁵ The mechanism behind the electroconvection has been intensively investigated in the last couple of decades. Rubinstein et al.²⁶ first suggested that a microvortex instability of the extended polarized region is responsible for the electroconvection. Theoretical^{27–29} and numerical^{30,31} studies showed that a strong electric field acting on an extended space charge region adjacent to the membrane can indeed destabilize the extended region and produce electroconvection. A nanochannel having ion-selective properties is often used to study processes associated with ion transport through ion-selective environments.^{7,30,32,33} Ion-selective nanochannels allowed the direct observation of electroconvection in the overlimiting region by fluorescence microscopy. These studies revealed the formation of a vortex array in front of a 1-mm-wide, 200-nm-high nanochannel and a pair of symmetrical vortices for a nanochannel with approximately the same width and height.³⁰ The mechanisms responsible for the occurrence of electroconvection due to the vortex instability were summarized in a review by Chang et al.³⁴

The membrane CVC dramatically changes when a second ion-exchange membrane having an opposite fixed charge is stacked onto the first one.^{35,36} Such a system can be compared to a semiconductor p-n-type junction, where one side of the junction is formed by a cation-exchange membrane enhancing the transport of cations and the other side is formed by an anion-exchange membrane with the anions as the major electrical current carriers. This system is known as a bipolar

membrane. Bipolar membranes, unlike monopolar ion-exchange membranes, behave like an ion diode with a strong rectification effect—the ion current is very different for forward and reverse biases.

The forward bias causes the formation of an ion-enriched region at the bipolar junction and exhibits a linear CVC ohmic curve. With reverse bias, the ions are depleted from the bipolar junction and the local electric field increases with decreasing ionic strength.³⁷ At a sufficiently high voltage, the electric field at the bipolar junction becomes sufficiently high to split water and the junction becomes an ionic reactor that continuously generates hydrogen cations and hydroxide anions (Figure 1, right).^{38–40} The resulting water-splitting current produces an overlimiting current that is higher than any other mechanism, including that due to electroconvection by the microvortex instability.

There has been interest in creating a bipolar membrane by adsorbing and functionalizing large polyelectrolytes with opposite charges onto the surface of an ion-selective membrane. It would be a simple means of synthesizing bipolar membranes with large ion currents, and the enhanced current could also be a sensitive reporter for the presence of surface fouling by biomolecules. Interestingly, the formation of a cationic layer either by adsorbed micelles containing monovalent benzalkonium chloride^{41,42} or by chemically introduced quaternary ammonium groups⁴³ on the surface of a cation-exchange membrane did not result in a water-splitting reaction when connected under reverse bias. In ref 43, the authors hypothesize that the absence of water splitting is caused by an absorbed micelle layer that can form a bipolar interface on the cation-exchange membrane without an intermediate layer of water. Conversely, Loza et al.⁴⁴ observed a decrease in the voltage corresponding to the onset of the overlimiting region for increasing coverage of a cation-exchange membrane with TBA^+ (tetrabutyl ammonium cations). The authors hypothesized without further investigation that this effect can be caused either by an enhanced water-splitting reaction due to the creation of local bipolar junctions or by enhanced electroconvection due to increased surface charge variation and heterogeneity. Because water splitting can corrupt the deionization efficiency of the membrane, considerable work has been devoted to removing it by immobilizing a thin layer having the same charge as the original membrane. These modifications have led to the almost complete elimination of the water-splitting reaction for both cation-⁴⁵ and anion-exchange membranes.⁴⁶

In this work, as a part of the development of new-generation DNA/RNA sensors, we conducted an in-depth study to explain and quantify the charge inversion required to form a bipolar membrane when large multivalent counterions are physisorbed onto a membrane surface. Specifically, we study the charge-inversion phenomenon on a heterogeneous anion-exchange membrane integrated into a microfluidic system in such a way that also allows us to perform pH fluorescence microscopy of the membrane surface. The heterogeneous anion-exchange membrane (Mega a.s., Czech republic) contains strongly basic and chemically stable quaternary ammonium groups bound to polystyrene/divinylbenzene particles that are embedded within a polyethylene matrix reinforced by polyamide or polyester fibers. Samples of single-stranded DNA (ssDNA) are used as large counterions. ssDNA molecules bear a negative charge at neutral pH because of the dissociation of hydrogen from phosphate groups that form the nucleic acid backbone. Phosphate groups on the DNA molecules are fully dissociated for the pH range of 4–8, with a pK_a of 2.0 for the conjugate acid of the DNA phosphate group.⁴⁷ We prepare four single-stranded ssDNA samples with different base lengths (29, 50, 75, and 100) to study the effects of the presence and ssDNA length on the experimentally obtained current–voltage characteristics. For simplicity, these four samples are denoted as DNA29, DNA50, DNA75, and DNA100. We then analyze the results and explain the behavior of the system with the use of real-time fluorescence microscopy of the membrane.

EXPERIMENTAL DETAILS

Reagents. PBS (Fisher Scientific, 10×) contained 1.37 M sodium chloride, 27 mM potassium chloride, 100 mM disodium hydrogen phosphate, and 18 mM potassium dihydrogen phosphate. PBS 0.1× used in the experiments was prepared by dilution from the PBS 10× solution. ssDNA (29, 50, 75, 100 bases, Invitrogen), fluorescein, rhodamine (Sigma-Aldrich), and a heterogeneous anion-exchange membrane containing strongly basic quaternary ammonium groups were provided by Mega a.s. (Czech Republic).

Microchip Fabrication. All experiments with the anion-exchange membrane were carried out in a microfluidic chip depicted in Figure 2a. The chip was designed as a two-channel system with four openings for electrolyte and sample loading and a small piece of an anion-exchange membrane bridging the two channels. The asymmetric channels are purposefully designed to measure CVCs as explained later. The basic dimensions of the chip are the following: size of the membrane, $1 \times 4 \text{ mm}^2$; size of the membrane exposed to the electrolyte in each channel, $1 \times 1 \text{ mm}^2$; height of the channel, 700 μm ; width of the channel, 2 to 4 mm; and total length of the channel, 14 mm. The fabrication of the microfluidic chip is based on PDMS cast against a glass/epoxy master containing fluidic structures on which a small piece of anion-exchange membrane was fixed with double-sided tape. The PDMS cast is then bonded to a glass slide by treatment with a hand-held corona discharge. Fluidic structures were designed in Adobe Illustrator and cut into a 700- μm -thick silicon sheet (having one sticky side) by using cutting plotter Graphtec Pro FC 7000MK2-60. A structured silicone sheet was fixed on a microscope slide, and the cut structures were filled with UV-curable glue (Loctite 3492).

After UV glue curing, we removed the silicon sheet, leaving the epoxy glue structures on the glass slide. A small piece of an anion-exchange membrane ($1 \times 4 \text{ mm}^2$) was then fixed at the designed locations on the master by using double-sided tape. PDMS prepolymer was prepared by mixing polymer base and curing agent in a weight ratio of 10:1 and degassing in vacuum. Four small pieces of silicon tubing serving as fluidic inlets and outlets were fixed on the master by using a small amount of PDMS prepolymer and curing it. PDMS prepolymer was then poured onto the whole master and degassed again. PDMS curing was done in an oven set at 70 °C for 40 min. The

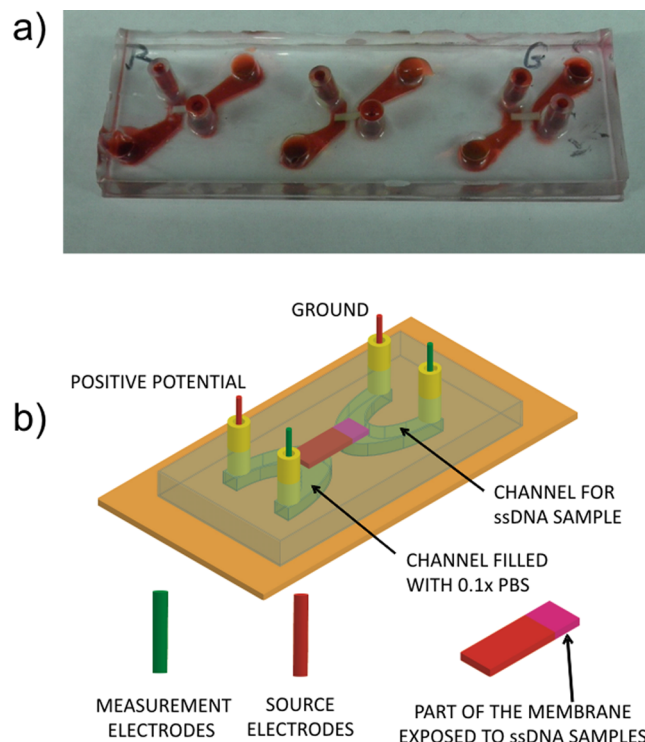


Figure 2. (a) Real chip with channels filled with rhodamine dye and (b) experimental connection of electrodes.

cured PDMS cast was peeled off of the master, and the double-sided tape was removed to expose the membrane in the cast channels. Any PDMS blocking inlet and outlet tubing was also removed. The PDMS cast was bonded to a precleaned glass slide using corona discharge followed by heating in an oven at 70 °C for 1 h. After bonding, we filled the channels with PBS 0.1× and allowed the membrane to swell for at least 48 h.

Measurement. All electrical measurements were made using a Gamry 500 potentiostat in a four-electrode setup. Two pseudosilver–silver chloride electrodes were used for the measurement of the actual voltage across the membranes, and two platinum electrodes were used to apply a current load. The whole experimental setup along with the position of the source and measurement electrodes is depicted in Figure 2b. The two measurement electrodes were placed in the channel openings close to the membrane, and the source electrodes were placed in the other two openings far from the membrane. This arrangement of electrodes provided accurate measurements of CVCs and allowed microscopic observation of the membrane surface with a minimum intervention of electrochemical reactions taking place on the source electrodes. One channel of the system was filled with PBS 0.1× solution, and the other one was used to inject DNA samples. The channel with the DNA sample was always connected to the ground whereas a positive potential was applied in the other channel. This connection ensured the formation of the depletion region in the channel with the DNA sample, making it very sensitive to the presence of DNA. To understand the exact mechanisms, we designed a few sets of experiments. In the first set, we measured the current–voltage characteristics of the anion-exchange membrane in the presence of four DNA samples with different concentrations. Different concentrations of each DNA sample were prepared by first dissolving the stock DNA powder in 1 mL of PBS 0.1× with subsequent dilution to the following concentrations: 0 nM, 1 nM, 10 nM, 100 nM, 250 nM, 500 nM, 1 μM , 5 μM , and 10 μM . The microfluidic chip was rinsed with PBS 0.1×, and then the channel on the sensing side of the membrane was filled with the DNA sample of a specific concentration and the CVC was measured immediately for each concentration. The current–voltage characteristics were measured by applying a current load from 0 to 80 μA at a rate of 1 $\mu\text{A}/\text{s}$. Voltage was measured with

measuring electrodes and recorded for each value of the applied current. The result of this measurement is plotted as the dependence of the electrical current on the measured voltage. Chronoamperometric curves were obtained by measuring the electrical current response of the system when the voltage on the measuring electrodes was kept constant and equal to 3 V for 180 s. We imaged the membrane surface with an inverted epifluorescence microscope (Olympus IX71) equipped with a mercury lamp from Olympus. Video was captured using a high-speed camera (Q-Imaging Retiga-EX) and with Streampix microscope software. The obtained videos were processed in a Matlab-based image-processing toolbox.

RESULTS

CVCs of the System with DNA. The qualitative effect of a DNA29 (29-base-long ssDNA in PBS 0.1×) sample with different concentrations on CVCs is shown in Figure 3a. The results for the other three samples (DNAS0, DNA75, and DNA100) are qualitatively similar and quantitatively evaluated in the next section.

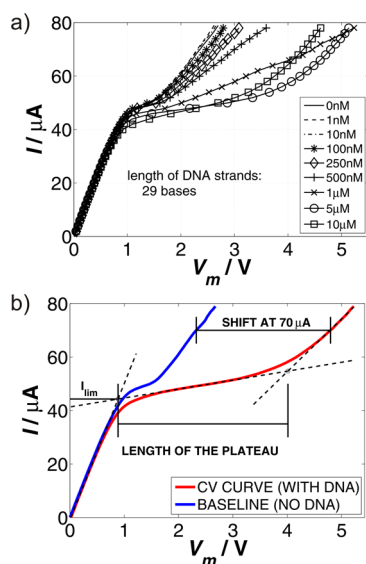


Figure 3. (a) CVCs of the system in the presence of different concentrations of DNA 29 sample in PBS 0.1×. (b) Parameters used for the quantitative description of CVCs for all DNA samples.

The CVCs for all concentrations of the DNA29 sample clearly bear the typical three-region characteristics where two linear regions (underlimiting and overlimiting) are connected to a limiting region. The underlimiting region of the measured CVCs in Figure 3a is same for all of the concentrations we tested. The main differences in the CVCs are seen for the limiting and overlimiting regions, which are strongly dependent on the DNA concentration. The CVCs for DNA concentrations of 1 and 10 nM are almost identical to the baseline, which is the CVC of our system with no DNA (PBS 0.1× only). The first detectable change occurs for the concentration of 100 nM, where the overlimiting region of the CVC slightly shifts away from the baseline. For concentrations larger than 100 nM (250 nM, 500 nM, and 1 μM), we observe that the overlimiting part of the CVC assumes smaller slopes with increasing DNA concentration causing this region to deviate significantly from the baseline. The same values of electrical currents are reached at larger voltages measured across the membrane, and we refer to this behavior as a shift of the CVC to the right. The CVC shift to the right, however, ceases at

DNA concentrations between 1 and 5 μM, when two effects happen at the same time: (i) the slope (differential conductance) of the overlimiting region starts to increase again and (ii) the limiting region extends significantly. For any higher DNA concentration (5 and 10 μM), the CVC changes character again by reducing the size of the LR and reducing the electrical current at which it starts to appear. This flip-flopping of CVCs with respect to increasing concentration of the DNA29 sample was surprising, but similar behavior is also observed for the other three DNA samples (DNAS0, DNA75, and DNA100). To get a better quantitative picture and a more coherent description of all of the DNA samples (DNA29, DNAS0, DNA75, and DNA100), we evaluated five parameters describing the CVCs for each DNA sample and concentration: (1) limiting electrical current, (2) length of the limiting region, (3) slope (differential conductance) of the limiting region, (4) shift in the voltage occurring at 70 μA with respect to the baseline, and (5) slope (differential conductance) of the overlimiting region. These parameters were evaluated in the following way (Figure 3b). First, linear regression was used to fit the three regions (underlimiting, limiting, and overlimiting) with their corresponding lines by analyzing the first 25 measured points (0–25 μA) for the underlimiting region and the last 15 points (65–80 μA) for the overlimiting region. The linear regression in the limiting region was done in a two-step process. We first found four consecutive points on the CVC that when fitted gave the smallest slope. We then used these four points for the linear regression of this region. All five parameters for the description of the CVCs can be easily extracted from these linear fits. The length of the limiting region was determined to be the distance between the intersection of the fit for the underlimiting and limiting regions and the intersection of the limiting and overlimiting regions.

Quantitative Description of CVCs. Figure 4a–e depicts the dependence of the five parameters on the concentration and length of the DNA strands. Qualitatively, the results show the same trend for all DNA samples; however, the highest or lowest values of a given parameter are reached at higher or lower DNA concentrations depending upon the length of the DNA strands. Samples containing shorter ssDNA reaches the maximum or minimum of the given parameter at higher concentration. The slope (differential conductance) of the CVC in the overlimiting region gives the information on the integral conductivity of the system, and thus it indirectly provides information on the effect of the negatively charged DNA molecules on the mechanisms responsible for the occurrence of the overlimiting current. As can be seen in Figure 4a, the addition of DNA to the sample results in a decrease in the slope in OR (overlimiting region), which suggests that the negatively charged DNA molecules suppresses the mechanism initially responsible for the overlimiting current. For all DNA samples, a minimum in the slope is observed; however, this minimum is reached for different concentrations in each sample: 1 μM for DNA29, 500 nM for DNAS0, 500 nM for DNA75, and 250 nM for DNA100. This observation clearly shows that longer DNA requires a smaller concentration to reach this minimum and shorter DNA requires a higher concentration. On further increases in the DNA concentration, the slope in the OR again starts to increase, which suggests that a new phenomenon is responsible for the increase in the conductance of the system. We denote the concentration at which a minimum slope in OR occurs as a critical concentration (C_c). The parameter characterizing the slope of CVC in the

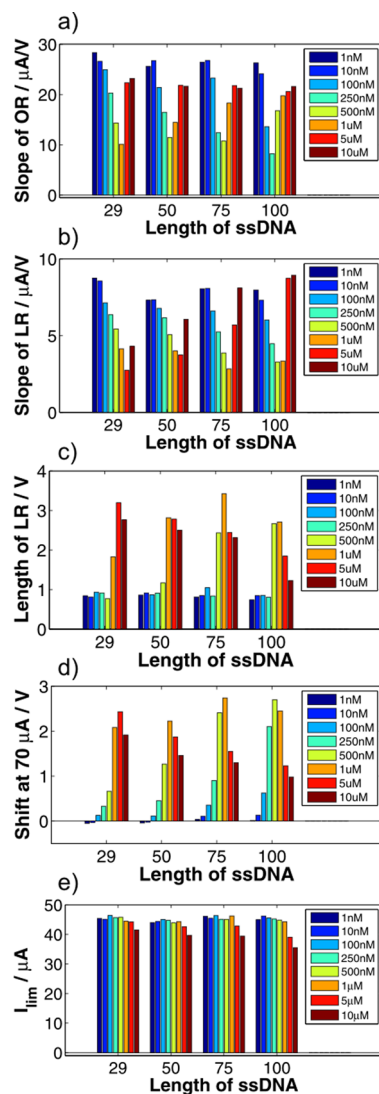


Figure 4. Bar graphs characterizing the CVCs quantitatively. The parameters plotted are (a) the slope of the OR, (b) the slope of the LR, (c) the length of the LR, (d) the shift at 70 μ A, and (e) the limiting current.

limiting region (Figure 4b) follows the same trend as the slope in OR (Figure 4a) (i.e., we can find a concentration for each DNA sample at which a minimum in the slope occurs). These concentrations are 5 μ M for DNA29, between 1 and 5 μ M for DNA50, 1 μ M for DNA75, and between 500 nM and 1 μ M for DNA100 and are larger than those obtained for the slope in the OR. This observation suggests that the process responsible for

the overlimiting current has its origin in the limiting region. The length of the limiting region is another interesting input in understanding the effects of DNA on the CVC (Figure 4c). Although the length of the limiting region is almost constant for DNA concentrations below the C_c , a sudden increase in the length of the limiting region around C_c is observed. This effect is especially profound for the DNA100 sample. A sudden increase in the length of the limiting region around C_c again indicates a change in the mechanisms driving the overlimiting current. The shift in the voltage occurring at 70 μ A (Figure 4d) has the opposite trend from the slope of the overlimiting region. First, it grows with increasing DNA concentration, reaches a maximum, and starts to decrease gradually. The concentrations at which the shift is maximal roughly coincide with the critical concentrations (C_c). This parameter is not assumed to be very important with respect to the understanding of the system behavior because its value is indirectly given by the length of the limiting region and the slope in the overlimiting region. The last parameter plotted in Figure 4e is the limiting current, which indicates at what current the limiting region starts. Because the limiting region is associated with the formation of the depletion region on the cathodic side of the membrane, it also provides information on how much current is needed to reach the depletion. Our results show that the limiting current is almost constant for concentrations smaller than C_c and decreases above C_c for all DNA samples.

These results again indicate that after reaching the critical concentration a mechanistic switch happens in our system and a new phenomenon starts to dominate in the OR.

Concentration of the Charge Bound to DNA Molecules Is the Determining Factor. The results in Figure 4a–e show that the DNA length has a profound effect on the CVCs. This is quite apparent in terms of the total negative charge borne by ssDNA molecules with different lengths. The longer the DNA molecule, the more phosphate groups available and the more negative the charge present in the sample. To understand our experimental results in terms of this negative charge (i.e., with respect to the total concentration of the phosphate groups or the charge concentration (assuming the full dissociation of all phosphate groups)), we plotted three of the five parameters evaluated above as a function of the concentration of phosphate groups (charge) for each DNA sample. These parameters are the slope of the LR (Figure 5a), the slope of the OR (Figure 5b), and the shift at 70 μ A (Figure 5c). As can be seen from these plots, the curves for the four DNA samples nicely collapse onto each other for all three parameters, showing a nice dependence of the system behavior on the concentration of the charge borne by DNA molecules independent of the DNA sample. We can also define the critical

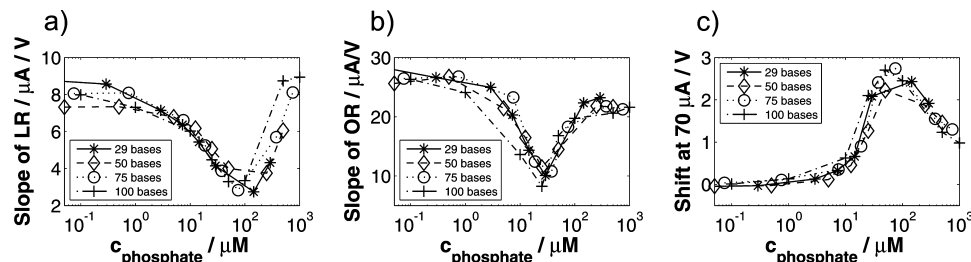


Figure 5. (a) slope of the LR, (b) slope of the OR, and (c) shift at 70 μ A plotted against the concentration of the phosphate groups bound to each DNA sample.

concentration of phosphate groups (charge concentration) as the concentration at which the conductivity in the overlimiting region drops to its lowest value, in other words, that at which the CVC slope in the overlimiting region reaches the smallest value. From Figure 5b, the value of the critical phosphate concentration is about $25 \mu\text{M}$. The plots in Figure 5 give clear evidence that the determining factor affecting the shape of the CVC is the concentration of the charge borne by the DNA molecules.

Direct Observation of Processes Occurring at the Membrane in the Overlimiting Region. In previous sections, we suggested two main competing mechanisms that control the overlimiting current for the concentrations above and below the critical concentration of the negative charge. We propose that the major mechanism that controls the overlimiting current for concentrations smaller than the C_c is electroconvection. By analyzing the experimental results of DNA concentration larger than C_c , we speculate that the negatively charged DNA molecules adsorb onto the positively charged membrane and create a bipolar junction that at sufficiently large voltages splits water. The overlimiting current is then given by the formation of new charge carriers, namely, H^+ and OH^- ions, in the water-splitting reaction. To prove that our hypothesis is correct, we perform real-time fluorescence microscopy measurements on the cathodic side of the membrane in the presence of DNA29 samples of different concentrations when an overlimiting voltage is applied to the system. We choose two fluorescent markers for our purposes: (i) fluorescein as a pH marker and (ii) rhodamine to capture any electroconvection. The fluorescence intensity of fluorescein is strongly affected by the pH of its environment.⁴⁸ It gives intensive fluorescent signal in neutral and alkaline solutions, but its fluorescence is completely lost in acidic solutions. Unlike fluorescein, the rhodamine fluorescence intensity does not show any significant dependence on the pH. In these experiments, the cathodic side of the membrane is observed during potentiometric measurements when 3 V is applied to the systems for 3 min. Five different concentrations of the DNA29 sample are tested: 0, 0.5, 1, 5, and $10 \mu\text{M}$.

pH Changes Occurring in the Presence of DNA. The results with fluorescein as the pH marker are plotted in Figure 6 and summarized in a movie (Movie1, Supporting Information). The frames capture the cathodic side of the membrane along with the channel leading to the platinum electrode connected as a cathode. Each column in Figure 6 shows the time evolution of a low-pH front in the cathodic channel for each DNA

concentration tested. The first column shows the situation when no DNA is present in the sample. In all frames captured, there is a large amount of green fluorescence coming from the whole channel on the cathodic side of the membrane. This observation confirms that when there are no large counterions the extent of water splitting (if any) is very low. The other four columns show the situation when a nonzero concentration of DNA is added to the sample. From the second to the fifth column, these concentrations are 0.5, 1, 5, and $10 \mu\text{M}$, respectively. For all DNA concentrations tested, we can see the formation of a zone with low fluorescence intensity. This low-fluorescence-intensity zone shows the change in the pH toward lower values, confirming the appearance of H^+ ions in the channel and their migration toward the cathode. The appearance of H^+ ions in the channel is very strong proof of the water-splitting reaction taking place on the membrane. The low-intensity zone appears at the membrane and extends farther into the channel with time. The extension of this low-intensity zone depends on the concentration of DNA. The higher the DNA concentration, the faster the generation of H^+ ions and hence the rapid broadening of that zone. In other words, the more DNA, the greater the number of H^+ ions generated at the membrane at the same external voltage applied in the range of DNA concentrations tested.

Electroconvection at the Membrane. The experiments with the rhodamine dye are carried out under experimental conditions similar to those for fluorescein (i.e., 3 V is applied to the system for 3 min, and five samples with different DNA concentrations (0, 0.5, 1, 5, and $10 \mu\text{M}$) are tested). The experimental results with rhodamine dye are summarized in Movie2 (Supporting Information) consisting of five frames showing the results for different DNA concentrations. The frames in the movie capture the situation occurring directly on the cathodic side of the membrane. When no DNA is present in the sample (the first frame), very intense vortices develop on the membrane surface shortly after the external voltage is applied. The intensity of the vortices does not change with time. This observation shows that the electroconvection can be responsible for the control of the overlimiting current by mixing the depletion region with a fresh electrolyte. The other four frames show the experimental results for DNA samples of different concentrations. From the second to the fifth column, these concentrations are 0.5, 1, 5, and $10 \mu\text{M}$, respectively. At $0.5 \mu\text{M}$ DNA, the vortices generated at the beginning of the movie are much less intense as compared to those for a system without any DNA. The vortices seem to disappear in the course of time, which might be given by the fact that more and more DNA molecules adsorb onto the membrane as a result of the action of the electrical field resulting in the suppression of vortices. For $1 \mu\text{M}$ DNA concentration, very low intensive whirling on the membrane is observed at the beginning of the experiment; however, after a short time, the vortices completely disappear again probably because of the increase in DNA concentration on the membrane surface. No detectable vortices are observed for 5 and $10 \mu\text{M}$ DNA concentrations. Overall, these movies show that there is very intensive mixing on the membrane surface for low DNA concentrations and no vortices are detected for high DNA concentrations. The change in intensity of the vortices is dependent on the DNA concentration.

The experimental results obtained for fluorescein and rhodamine dyes can be summarized as the following: (i) the vortices appear very quickly on the membrane when there is no

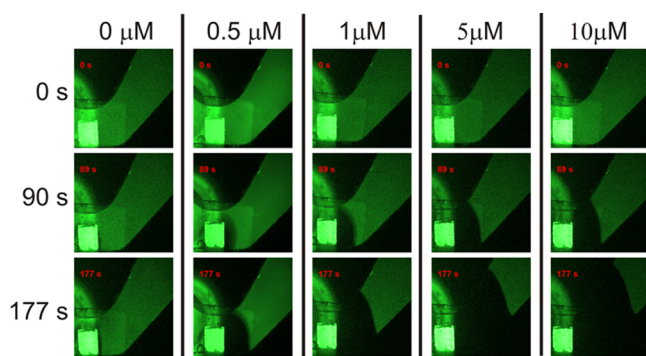


Figure 6. Evolution of the low-pH zone at different concentrations of the DNA29 sample. From left to right, the concentrations in the columns are 0, 0.5, 1, 5, and $10 \mu\text{M}$, respectively.

DNA present in the solution, (ii) the intensity of the vortices decreases with increasing concentration of DNA and become undetectable for high concentrations of DNA, (iii) the extent of pH change in the channel on the cathodic side of the membrane caused by the water-splitting reaction depends on the concentration of DNA, and (iv) there is almost no pH change detectable when no DNA is present in the sample. Another interesting conclusion can be made with respect to our critical concentration of DNA. We determine this concentration to be about $25 \mu\text{M}$ for phosphate groups, which gives a roughly $1 \mu\text{M}$ concentration for the DNA29 sample. At this concentration, we can detect vortices of a very low intensity whereas the extent of the water-splitting reaction starts to dominate. Therefore, we consider this concentration to separate the regions of vortex-controlled and water-splitting-controlled overlimiting currents in our system.

Chronoamperometry Curves in the Presence of DNA. Figure 7 shows the chronoamperometric curves obtained for

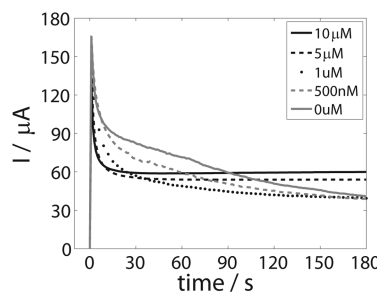


Figure 7. Chronoamperometric curves obtained for different concentrations of the DNA29 sample.

the experiments to explore the overlimiting current mechanism further. The presence of ssDNA has a profound effect on chronoamperometric curves at the beginning of the experiment when the depletion zone is created and at steady state when the overlimiting current fully sets in. At all DNA concentrations, the current reaches a maximum value, right after the voltage is activated, followed by a sharp decrease (0–10 s) and then some slower evolution. The sharp decrease is associated with the formation of the depletion region and is faster for higher DNA concentrations. Beyond the sharp decrease, the current at low DNA concentrations ($0 \mu\text{M}$, solid gray line; 500 nM , dashed gray line) does not reach a steady value and slowly decreases for the entire experiment. In contrast, the ionic current reaches a steady-state value at around $60 \mu\text{A}$ for high DNA concentrations ($5 \mu\text{M}$, dashed black line; $10 \mu\text{M}$, solid black line). The curve for $1 \mu\text{M}$ DNA (dotted black line) creates a transition between low and high DNA concentrations. This observation again confirms our hypothesis for the switch in mechanism for the OR current. At low DNA concentrations (below $1 \mu\text{M}$) when vortices are suggested to be the major mechanism for OR, the current slowly but steadily decreases, which reflects a slow decrease in the ion concentration in the bulk. This is in agreement with the fact that the ion concentration slowly decreases (ionic conductivity decreases) on the depletion side of the membrane and some of the ions are even consumed in electrochemical reactions on the electrodes (e.g., Cl^- forms chlorine). In contrast, at high DNA concentration the ionic current reaches a steady value that is slightly higher for the $10 \mu\text{M}$ DNA solution. The ability of the system to keep the ionic current constant strongly

suggests that a new constant source of ions sets in to suppress further ion concentration decreases. Along with the low-pH zone that is observed in the videos in Figure 6 at high DNA concentration, this proves that the water-splitting reaction controls the OR current with large DNA coverage. Again, the concentration of $1 \mu\text{M}$ separates the vortex-controlled and water-splitting-controlled OR.

Principal Component Analysis of Vortices. To quantify the correlation between electroconvection and the ion current better, we carried out principal component analysis (PCA) of the movies capturing the vortices developed on the membrane surface using the procedure described by Chang et al.⁴⁹ By using PCA analysis, we examine the short-time ensemble average of the correlation between the fluorescence intensity of any two pixels in the image, which has been reduced with respect to the mean over the same time interval. The PCA analysis offers a set of statistically uncorrelated eigenimages from the cross-correlation study, with the first one representing the most dominant and correlated intensity fluctuation in time as a result of coherent vortices. The first principal component of this leading eigenimage can hence measure the intensity of the vortex motion. We calculate the dependence of the first principal component coefficient (a_1) on time (on a time scale longer than that used for the ensemble average) and use its power spectrum to examine the frequency signature of the vortices. At the same time, we calculate power spectra of the current signal that was recorded during the measurement subtracted from the current mean and compare these power spectra to those produced for a_1 (Figure 8) for four different ssDNA concentrations (crosses:, $5 \mu\text{M}$; circles, $1 \mu\text{M}$; diamonds, $0.5 \mu\text{M}$; and squares, $0 \mu\text{M}$).

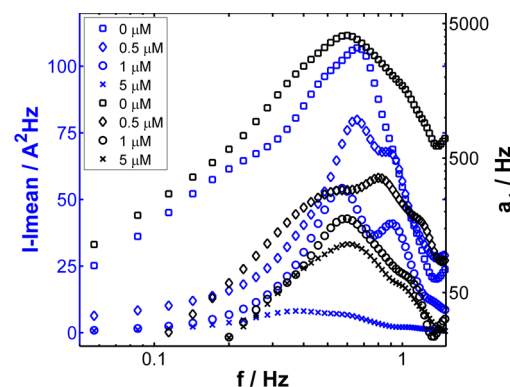


Figure 8. Power spectra of the current (blue curves) and the first principal coefficient (black curves) for different DNA concentrations: squares, $0 \mu\text{M}$; diamonds, $0.5 \mu\text{M}$; circle, $1 \mu\text{M}$, and crosses, $5 \mu\text{M}$.

We can see that for a bare membrane we get a maximum in the power spectra of both a_1 and the current for frequencies of around 0.6 to 0.7 Hz. With increasing concentrations of DNA (0.5 and $1 \mu\text{M}$), the maximum in the spectra decreases but the position of the maximum remains essentially constant. The decrease in the maxima clearly shows that the DNA molecules, even at rather small concentrations, have a profound damping effect on both the current and fluorescence intensity fluctuations. For the highest DNA concentration ($5 \mu\text{M}$), the peak is almost completely lost, indicating very small fluctuations in the current and fluorescence intensity. These results are in very good agreement with the visual analysis of Movie2 described earlier. Vortices can hence be correlated with the

passage of an electrical current through the membrane with respect to both their mean values and their fluctuation intensities.

■ DISCUSSION

By performing the experiments above, we have shown two main mechanisms that govern the overlimiting current at an anion-exchange membrane in the presence of large counterions. These two mechanisms are electroconvection and the water-splitting reaction. We found that the importance of each of the mechanisms is dependent on the concentration of DNA molecules, which was further shown to be primarily given by the concentration of the negative charge borne by these molecules. Because electroconvection has been suggested to result from the instability of a surface-extended polarized region with a space charge whose dimension is no larger than 100 nm,^{27,29,50} the presence of ssDNA on the surface is expected to reduce the slip length or increase the viscous dissipation in the polarized layer significantly such that the intensities of the vortices and electroconvection are reduced. This effective viscous effect seems to exist at low ssDNA coverage. The scenario changes when ssDNA forms a cation-selective membrane on the original membrane beyond a critical concentration of negative charges borne by the DNA molecules. Our pH-sensitive fluorescence imaging suggests the formation of a proton front sustained by protons generated by water splitting at the DNA/membrane junction. The large pH and ion-current signatures of the water-splitting reaction at large DNA coverage suggests that it can be used to detect and quantify large counterion polyelectrolytes on the membrane surface. Currently, ssDNA adsorbs on the surface, but we expect the same vortex-suppression and water-splitting phenomena to exist when specific ssDNA or ssRNA hybridizes onto short probes functionalized on the membrane surface. Nonspecific binding will be an issue, but as shown earlier,⁵¹ hydrodynamic shear and alkaline shocking⁵² can be used to remove nonspecifically bound molecules on the membrane surface. Although the current signatures resemble those for electrochemical conductivity sensors, the current and voltage signals and changes are much larger, thus allowing more sensitive measurement with simpler instrumentation and much lower material cost. The new membrane sensor also does not require redox reporters to enhance the signal and is not sensitive to spurious electrochemical reactions; therefore, there is no electron-transfer reaction involved.

■ ASSOCIATED CONTENT

Supporting Information

Movies capturing pH changes (Movie1) and electroconvection (Movie2). This material is available free of charge via the Internet at <http://pubs.acs.org>.

■ AUTHOR INFORMATION

Corresponding Author

*E-mail: hchang@nd.edu.

Author Contributions

Z.S. designed and carried out the experiments, analyzed the data, and wrote the manuscript. S.S. analyzed the data and wrote the manuscript. Y.Y. performed PCA analysis and power spectra analysis. H.-C.C. analyzed the data and wrote the manuscript.

Notes

The authors declare no competing financial interest.

■ ACKNOWLEDGMENTS

This work is supported by NSF CBET 1065652 and USDA grant 2012-67005-19589.

■ ABBREVIATIONS

CVC, current–voltage characteristics; LR, limiting region; OR, overlimiting region; DNA, DNA; ssDNA, single stranded DNA

■ REFERENCES

- (1) Xu, T. Ion Exchange Membranes: State of Their Development and Perspective. *J. Membr. Sci.* **2005**, *263*, 1–29.
- (2) Rubinstein, I.; Shtilman, L. Voltage against Current Curves of Cation-Exchange Membranes. *J. Chem. Soc., Faraday Trans. 2* **1979**, *75*, 231–246.
- (3) Barragan, V. M.; Ruiz-Bauza, C. Current-Voltage Curves for Ion-Exchange Membranes: A Method for Determining the Limiting Current Density. *J. Colloid Interface Sci.* **1998**, *205*, 365–373.
- (4) Levich, V. G. *Physicochemical Hydrodynamics*; Prentice-Hall: Englewood Cliffs, NJ, 1962; p 700.
- (5) Tanaka, Y. Concentration Polarization in Ion-Exchange Membrane Electrodialysis. The Events Arising in an Unforced Flowing Solution in a Desalting Cell. *J. Membr. Sci.* **2004**, *244*, 1–16.
- (6) Ben, Y.; Chang, H. C. Nonlinear Smoluchowski Slip Velocity and Micro-Vortex Generation. *J. Fluid Mech.* **2002**, *461*, 229–238.
- (7) Yossifon, G.; Mushenheim, P.; Chang, Y. C.; Chang, H. C. Nonlinear Current-Voltage Characteristics of Nanochannels. *Phys. Rev. E* **2009**, *79*, 4.
- (8) Kooistra, W. Characterization of Ion Exchange Membranes by Polarization Curves. *Desalination* **1967**, *2*, 139–147.
- (9) Frilette, V. J. Electrogravitational Transport at Synthetic Ion Exchange Membrane Surfaces. *J. Phys. Chem.* **1957**, *61*, 168–174.
- (10) Andersen, M. B.; van Soestbergen, M.; Mani, A.; Bruus, H.; Biesheuvel, P. M.; Bazant, M. Z. Current-Induced Membrane Discharge. *Phys. Rev. Lett.* **2012**, *109*, 10.
- (11) Krol, J. J.; Wessling, M.; Strathmann, H. Concentration Polarization with Monopolar Ion Exchange Membranes: Current-Voltage Curves and Water Dissociation. *J. Membr. Sci.* **1999**, *162*, 145–154.
- (12) Belova, E. I.; Lopatkova, G. Y.; Pismenskaya, N. D.; Nikonenko, V. V.; Larchet, C.; Pourcelly, G. Effect of Anion-Exchange Membrane Surface Properties on Mechanisms of Overlimiting Mass Transfer. *J. Phys. Chem. B* **2006**, *110*, 13458–13469.
- (13) Zabolotsky, V. I.; Nikonenko, V. V.; Pismenskaya, N. D. On the Role of Gravitational Convection in the Transfer Enhancement of Salt Ions in the Course of Dilute Solution Electrodialysis. *J. Membr. Sci.* **1996**, *119*, 171–181.
- (14) Dydek, E. V.; Zaltzman, B.; Rubinstein, I.; Deng, D. S.; Mani, A.; Bazant, M. Z. Overlimiting Current in a Microchannel. *Phys. Rev. Lett.* **2011**, *107*, 11.
- (15) Mani, A.; Bazant, M. Z. Deionization Shocks in Microstructures. *Phys. Rev. E* **2011**, *84*, 6.
- (16) Belova, E.; Lopatkova, G.; Pismenskaya, N.; Nikonenko, V.; Larchet, C. Role of Water Splitting in Development in Ion-Exchange Membrane of Electroconvection Systems. *Desalination* **2006**, *199*, 59–61.
- (17) Pismenskaya, N. D.; Nikonenko, V. V.; Belova, E. I.; Lopatkova, G. Y.; Sistat, P.; Pourcelly, G.; Larshe, K. Coupled Convection of Solution near the Surface of Ion-Exchange Membranes in Intensive Current Regimes. *Russ. J. Electrochem.* **2007**, *43*, 307–327.
- (18) Rosler, H. W.; Maletzki, F.; Staude, E. Ion Transfer across Electrodialysis Membranes in the Overlimiting Current Range - Chronopotentiometric Studies. *J. Membr. Sci.* **1992**, *72*, 171–179.
- (19) Maletzki, F.; Rosler, H. W.; Staude, E. Ion Transfer across Electrodialysis Membranes in the Overlimiting Current Range - Stationary Voltage Current Characteristics and Current Noise Power Spectra under Different Conditions of Free-Convection. *J. Membr. Sci.* **1992**, *71*, 105–115.

- (20) Krol, J. J.; Wessling, M.; Strathmann, H. Chronopotentiometry and Overlimiting Ion Transport through Monopolar Ion Exchange Membranes. *J. Membr. Sci.* **1999**, *162*, 155–164.
- (21) Kang, M. S.; Choi, Y. J.; Moon, S. H. Effects of Charge Density on Water Splitting at Cation-Exchange Membrane Surface in the Over-Limiting Current Region. *Korean J. Chem. Eng.* **2004**, *21*, 221–229.
- (22) Belashova, E. D.; Melnik, N. A.; Pismenskaya, N. D.; Shevtsova, K. A.; Nebavsky, A. V.; Lebedev, K. A.; Nikonenko, V. V. Overlimiting Mass Transfer through Cation-Exchange Membranes Modified by Nafion Film and Carbon Nanotubes. *Electrochim. Acta* **2012**, *59*, 412–423.
- (23) Volodina, E.; Pismenskaya, N.; Nikonenko, V.; Larchet, C.; Pourcelly, G. Ion Transfer Across Ion-Exchange Membranes with Homogeneous and Heterogeneous Surfaces. *J. Colloid Interface Sci.* **2005**, *285*, 247–258.
- (24) Choi, J. H.; Kim, S. H.; Moon, S. H. Heterogeneity of Ion-Exchange Membranes: The Effects of Membrane Heterogeneity on Transport Properties. *J. Colloid Interface Sci.* **2001**, *241*, 120–126.
- (25) Choi, J.-H.; Lee, H.-J.; Moon, S.-H. Effects of Electrolytes on the Transport Phenomena in a Cation-Exchange Membrane. *J. Colloid Interface Sci.* **2001**, *238*, 188–195.
- (26) Rubinstein, I.; Staude, E.; Kedem, O. Role of the Membrane-Surface in Concentration Polarization at Ion-Exchange Membrane. *Desalination* **1988**, *69*, 101–114.
- (27) Rubinstein, I.; Zaltzman, B. Extended Space Charge in Concentration Polarization. *Adv. Colloid Interface Sci.* **2010**, *159*, 117–129.
- (28) Zaltzman, B.; Rubinstein, I. Electro-Osmotic Slip and Electroconvective Instability. *J. Fluid Mech.* **2007**, *579*, 173–226.
- (29) Kim, Y.; Lawler, D. F. Overlimiting Current by Interactive Ionic Transport between Space Charge Region and Electric Double Layer near Ion-Exchange Membranes. *Desalination* **2012**, *285*, 245–252.
- (30) Yossifon, G.; Mushenheim, P.; Chang, Y. C.; Chang, H. C. Eliminating the Limiting-Current Phenomenon by Geometric Field Focusing into Nanopores and Nanoslots. *Phys. Rev. E* **2010**, *81*, 4.
- (31) Postler, T.; Slouka, Z.; Svoboda, M.; Pribyl, M.; Snita, D. Parametrical Studies of Electroosmotic Transport Characteristics in Submicrometer Channels. *J. Colloid Interface Sci.* **2008**, *320*, 321–332.
- (32) Kim, S. J.; Wang, Y. C.; Lee, J. H.; Jang, H.; Han, J. Concentration Polarization and Nonlinear Electrokinetic Flow near a Nanofluidic Channel. *Phys. Rev. Lett.* **2007**, *99*, 4.
- (33) Yossifon, G.; Mushenheim, P.; Chang, H. C. Controlling Nanoslot Overlimiting Current with the Depth of a Connecting Microchamber. *Euro. Phys. Lett.* **2010**, *90*, 6.
- (34) Chang, H. C.; Yossifon, G.; Demekhin, E. A. Nanoscale Electrokinetics and Microvortices: How Microhydrodynamics Affects Nanofluidic Ion Flux. *Annu. Rev. Fluid Mechanics* **2012**, *44*, 401–.
- (35) Strathmann, H.; Krol, J. J.; Rapp, H. J.; Eigenberger, G. Limiting Current Density and Water Dissociation in Bipolar Membranes. *J. Membr. Sci.* **1997**, *125*, 123–.
- (36) Ramirez, P.; Rapp, H. J.; Mafe, S.; Bauer, B. Bipolar Membranes under Forward and Reverse Bias Conditions - Theory vs Experiment. *J. Electroanal. Chem.* **1994**, *375*, 101–.
- (37) Conroy, D. T.; Craster, R. V.; Matar, O. K.; Cheng, L. J.; Chang, H. C. Nonequilibrium Hysteresis and Wien Effect Water Dissociation at a Bipolar Membrane. *Phys. Rev. E* **2012**, *86*, 5.
- (38) Desharnais, B. M.; Lewis, B. A. G. Electrochemical Water Splitting at Bipolar Interfaces of Ion Exchange Membranes and soils. *Soil Sci. Soc. Am. J.* **2002**, *66*, 1518.
- (39) Aritomi, T.; van den Boomgaard, T.; Strathmann, H. Current-Voltage Curve of a Bipolar Membrane at High Current Density. *Desalination* **1996**, *104*, 13–.
- (40) Cheng, L. J.; Chang, H. C. Microscale pH Regulation by Splitting Water. *Biomicrofluidics* **2011**, *5*, 46502.
- (41) Suendo, V.; Eto, R.; Tanioka, A. Ionic Rectification Properties of a Bipolar Interface Consisting of a Cationic Surfactant and Cation-Exchange Membrane. *J. Colloid Interface Sci.* **2002**, *250*, 507–.
- (42) Suendo, V.; Minagawa, M.; Tanioka, A. Bipolar Interface Formation of Cationic Surfactant on the Surface of a Cation-Exchange Membrane: Current-Voltage Characteristics in Aqueous Electrolyte Solution. *Langmuir* **2002**, *18*, 6266–.
- (43) Chamoulaud, G.; Belanger, D. Modification of Ion-Exchange Membrane Used for Separation of Protons and Metallic Cations and Characterization of the Membrane by Current-Voltage Curves. *J. Colloid Interface Sci.* **2005**, *281*, 179–.
- (44) Loza, N. V.; Kononenko, N. A.; Shkirskaya, S. A.; Berezina, N. P. Effect of Modification of Ion-Exchange Membrane MF-4SK on Its Polarization Characteristics. *Russ. J. Electrochem.* **2006**, *42*, 815–.
- (45) Sharafan, M. V.; Zabolotskii, V. I.; Bugakov, V. V. Electric mass transport through homogeneous and surface-modified heterogeneous ion-exchange membranes at a rotating membrane disk. *Russ. J. Electrochem.* **2009**, *45*, 1162.
- (46) Lopatkova, G. Y.; Volodina, E. I.; Pis'menskaya, N. D.; Fedotov, Y. A.; Cot, D.; Nikonenko, V. V. Effect of Chemical Modification of Ion-Exchange Membrane MA-40 on Its Electrochemical Characteristics. *Russ. J. Electrochem.* **2006**, *42*, 847–.
- (47) Inoshita, S.; Tsukahara, S.; Fujiwara, T. In Situ Fluorescence Microscopic Investigation into the Dependence of Conformation and Electrophoretic Velocity of Single DNA Molecules on Acid or Spermidine Concentration. *Anal. Sci.* **2009**, *25*, 293–.
- (48) Doughty, M. J. pH Dependent Spectral Properties of Sodium Fluorescein Ophthalmic Solutions Revisited. *Ophthalmic Physiol. Opt.* **2010**, *30*, 167–.
- (49) Chen, C. C.; Wolf, E. E.; Chang, H. C. Low-Dimensional Spatiotemporal Thermal Dynamics on Nonuniform Catalytic Surfaces. *J. Phys. Chem.* **1993**, *97*, 1055–.
- (50) Rubinstein, I.; Maletzki, F. Electroconvection at an Electrically Inhomogeneous Permselective Membrane-Surface. *J. Chem. Soc., Faraday Trans.* **1991**, *87*, 2079–.
- (51) Cheng, I. F.; Froude, V. E.; Zhu, Y. X.; Chang, H. C.; Chang, H. C. A Continuous High-Throughput Bioparticle Sorter Based on 3D Traveling-Wave Dielectrophoresis. *Lab Chip* **2009**, *9*, 3193–.
- (52) Basuray, S.; Senapati, S.; Ajian, A.; Mahon, A. R.; Chang, H. C. Shear and AC Field Enhanced Carbon Nanotube Impedance Assay for Rapid, Sensitive, and Mismatch-Discriminating DNA Hybridization. *ACS Nano* **2009**, *3*, 1823.